Communication

Anomalous α-Mg Dendrite Growth During Directional Solidification of a Mg-Zn Alloy

SANSAN SHUAI, ENYU GUO, MINGYUE WANG, MARK D. CALLAGHAN, TAO JING, QIWEI ZHENG, and PETER D. LEE

Dendritic morphology was investigated in a directionally solidified magnesium-zinc alloy using synchrotron X-ray tomography and electron backscattered diffraction. Unexpectedly, primary dendrites grew along $\langle 21\bar{3}1\rangle$, rather than the previously reported $\langle 11\bar{2}0\rangle$ and $\langle 22\bar{4}5\rangle$ directions. Further, seven asymmetric sets of side branches formed, instead of six-fold symmetric arms, evolving with three coexisting morphologies per trunk of: traditional, seaweed structure, and free growth. The anomalous growth is attributed to the imposed thermal gradient and zinc-induced interfacial energy anisotropy variations.

DOI: 10.1007/s11661-016-3618-0

Magnesium alloys are gaining increasing attention for use as structural components in the automotive and aerospace sectors[1–3] due to their low density and high strength-to-weight ratio. Understanding and controlling microstructural evolution in Mg alloys, including dendritic growth orientation and morphology during solidification, is critical to obtaining optimal mechanical properties.[4] Microtomography has proven to be a powerful tool for investigating dendritic growth and morphology for bcc and fcc alloys, with prior studies primarily focussed on binary aluminum alloys containing copper[5–7] or zinc,[8–10] which grow with a preferred orientation of [100] and form a four-fold symmetric structure.[4,11]

Mg alloys are hcp, with a crystal structure that has six-fold symmetry. Many prior metallographic experimental studies, and simulations, have shown that the primary α-Mg dendrites grow with a preferred direction of $\langle 11\bar{2}0\rangle$, as reported in References 12 through 14 for Mg-9wt pctAl alloys and for Mg-40wt pctZn.[15] The growth direction of $\langle 22\bar{4}5\rangle$ and $\langle 11\bar{2}1\langle$ have also been reported under some conditions in Mg alloys.[15–18]

However, a number of recent studies in aluminum alloys have shown that the growth direction and dendrite morphology in metallic alloy systems can be altered from the expected value. The two most common ways to achieve new microstructure are as follows: 1. the addition of alloying elements, which significantly alter the interfacial surface tension anisotropy, γ'_{sl}; 2. imposed thermal conditions (thermal gradient, G, and growth velocity, V). Rappaz *et al.*[8–10,19] demonstrated that the addition of Zn alters the preferred growth direction in aluminum alloys, transforming α-Al dendrites from $\langle 100\rangle$ to $\langle 110\rangle$ as the Zn wt pct is increased from 5 to 90 pct. The addition of Zn to Al is thought to strongly increase γ'_{sl}. Although this change in the γ'_{sl} of Al with increasing Zn has not been experimentally quantified, the anisotropy has been shown to be low (typically 1 pct) between the [001] and [011] directions in dilute Al-Cu, Al-Si,[20] and Al-Sn[21] binary alloys. In contrast, the anisotropy in hcp zinc is very large, as high as 30 pct between the *c*-direction and the growth directions in the basal plane.[9,10] Based on this, Rappaz *et al.* hypothesized that the addition of Zn increased the anisotropy causing a dendrite orientation transition[8–10,19] in Al alloys. In terms of the influence of imposed thermal conditions, Pettersen *et al.*[16,17] demonstrated that the growth direction of primary α-Mg dendrites in a directionally solidified (DS) AZ91 alloy (90.8Mg-8.25Al-0.7Zn-0.35Mn, wt pct) could be altered from $\langle 11\bar{2}0\rangle$ at low G and high V to $\langle 22\bar{4}5\rangle$ for high G and low V. In addition, the number of secondary arm side branches transformed from the expected six to only three. Together, these studies suggest that both the influence of alloying and the imposed solidification conditions must be considered when predicting dendritic growth.

Like aluminum, magnesium has been reported to have a weak interfacial anisotropy, especially between the *c*-axis and basal plane.[22,23] Therefore, investigating the influence of an alloying element with a high intrinsic γ'_{sl} on the formation of α-Mg dendrites is of interest to determine if this element can be used to control the structure. Zinc is one such addition, as it has a similar hcp structure but a very strong γ'_{sl}. In the present study,

SANSAN SHUAI, Ph.D Student, is with the Key Laboratory for Advanced Materials Processing Technology, Ministry of Education, School of Materials Science and Engineering, Tsinghua University, Beijing 100084, P.R.China, and also with the School of Materials, The University of Manchester, Oxford Road, Manchester M13 9PL, U.K. ENYU GUO and MARK D. CALLAGHAN, Research Associates, and PETER D. LEE, Professor, are with the School of Materials, The University of Manchester. Contact e-mail: peter.lee@manchester.ac.uk MINGYUE WANG, Postdoctoral Researcher, is with the International Research Institute for Multidisciplinary Science, Beihang University, Beijing 100191, China. TAO JING, Professor, and QIWEI ZHENG, Master Student, are with the Key Laboratory for Advanced Materials Processing Technology, Ministry of Education, School of Materials Science and Engineering, Tsinghua University. Contact e-mail: jingtao@mail.tsinghua.edu.cn.

Manuscript submitted March 8, 2016.
Article published online July 8, 2016

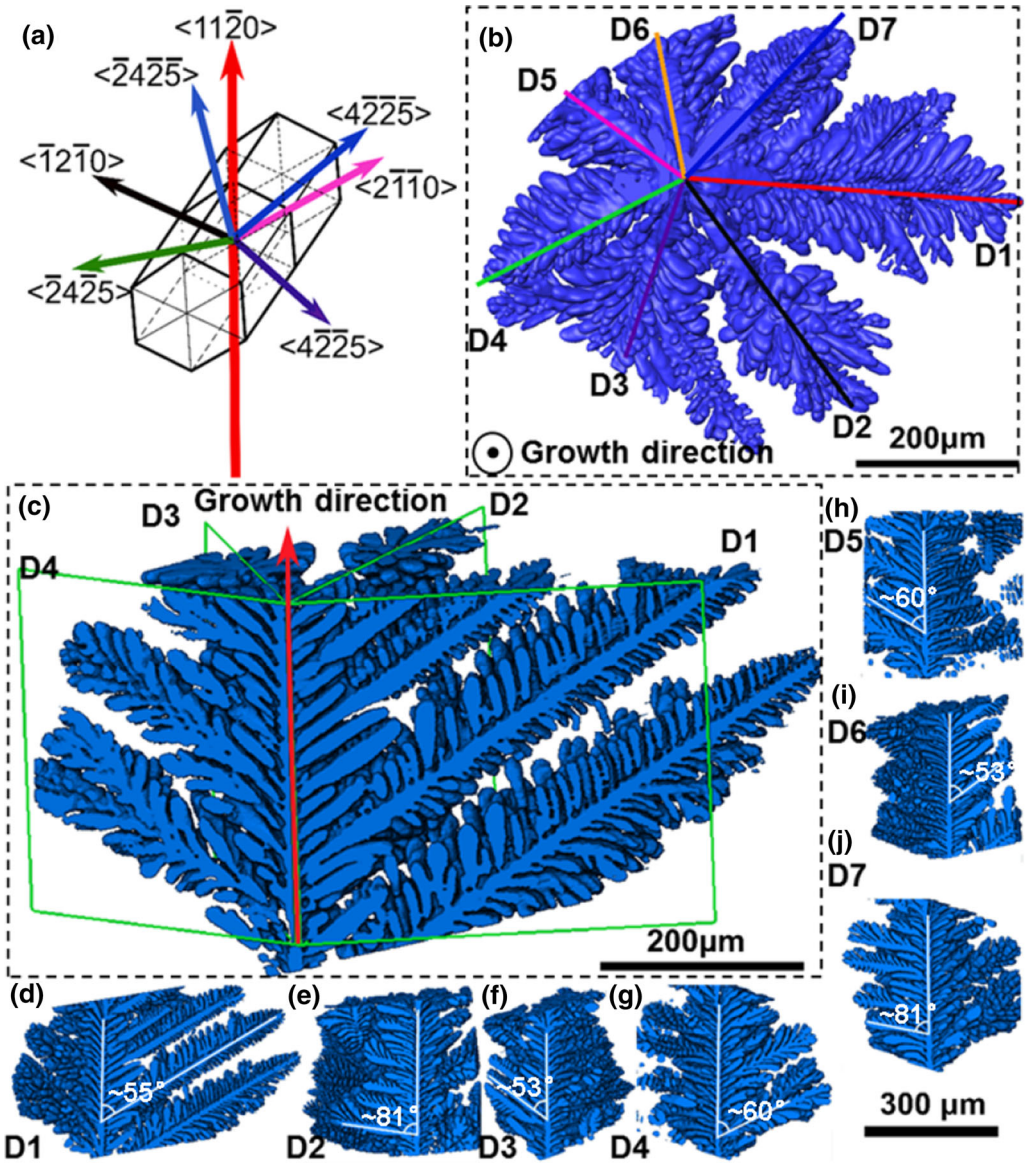

Fig. 1—Segmented primary α-Mg columnar dendrite and its secondary arms from sCT tomogram of a directionally solidified Mg-38wt pct alloy. (*a*) Expected six-fold crystallography and growth directions (as observed previously in DS AZ91[16]); (*b*) 3D rendering of the seven secondary arm side branches (marked D1-7, growth direction into the page; (*c*) primary dendrite oriented in the vertical direction; (*d* through *j*) morphologies of each of the seven secondary arms side branches and their angles relative to the stem (d, f, i-~54°; e, j-~81°; g, h-~60°). (d-j have the same scale).

Table I. Measured Angles (Degree, °) Between Seven Secondary Arms (SA) and the Primary Trunk

	D1	D2	D3	D4	D5	D6	D7
Dendrite1							
Min	55.0	81.4	53.8	58.3	58.7	53.5	79.3
Max	56.6	82.1	54.8	61.4	62.1	53.9	81.3
Avg. (Var.)	55.6 (0.4)	81.8 (2.7)	54.3 (0.2)	60.2 (1.7)	61.2 (1.9)	53.7 (0.02)	80.3 (0.7)
Dendrite2							
Min	52.1	76.3	51.8	57.9	58.5	51.3	77.8
Max	54.9	82.5	54.1	63.8	62.5	56.3	82.3
Avg. (Var.)	53.9 (0.8)	80.5 (3.9)	52.8 (0.5)	61.1 (3.6)	61 (1.8)	54.3 (1.2)	80.5 (1.4)
Dendrite3							
Min	52.5	77.2	50.6	59.5	59.5	53.2	79
Max	55.6	83.3	54.2	66.1	63.0	55.5	82
Avg. (Var.)	54.1 (0.6)	80.8 (3.1)	52.6 (1.0)	62.1 (4.2)	61.4 (1.2)	54.4 (0.4)	80.6 (0.9)

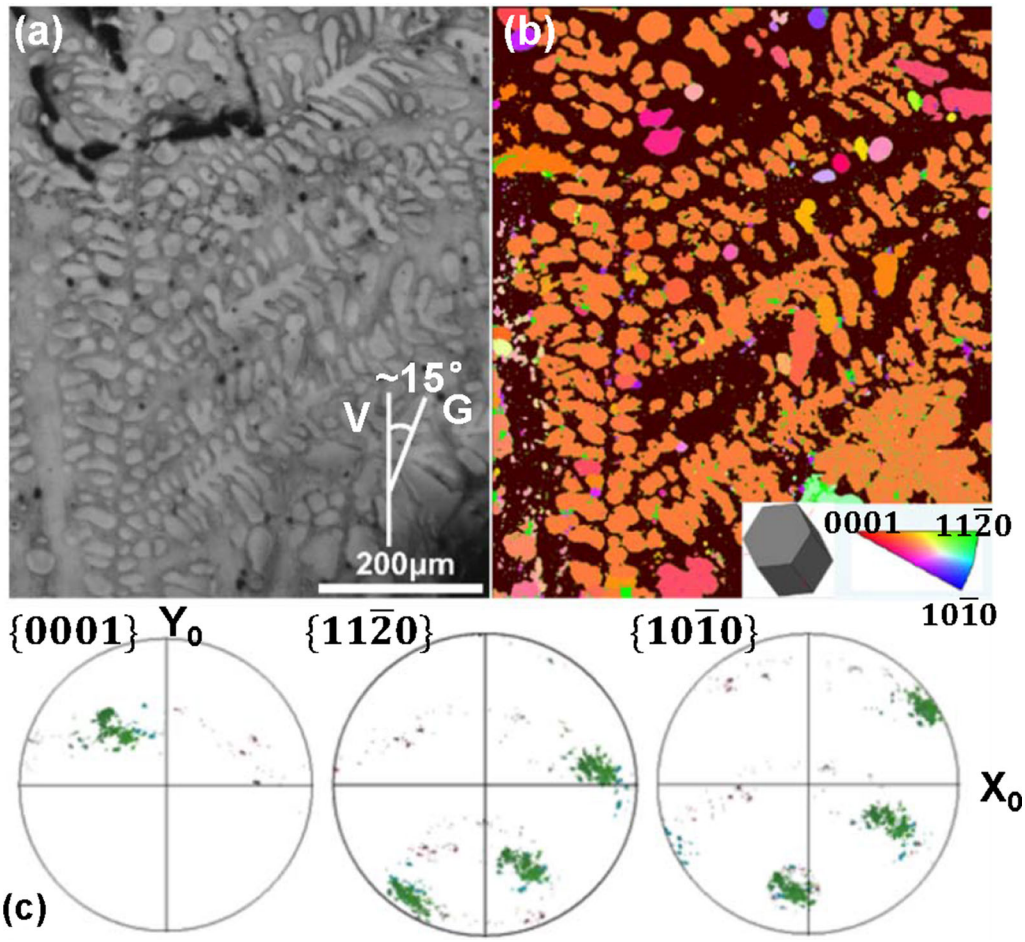

Fig. 2—(*a*) Backscattered electron (BSE) micrograph and (*b*) EBSD orientation map on a longitudinal section of the secondary arm side branch; (*c*) Pole figure of the primary dendrite. (Note, in (a), *G* is the thermal gradient and *V* the growth direction of the primary dendrite. In (b), black represents the unanalysed eutectic.).

the effect of Zn on the growth direction of α-Mg dendrites has been investigated using synchrotron X-ray tomography (sCT) and electron backscattered diffraction (EBSD).

For this experiment, a Mg-38wt pctZn alloy was produced and then directionally solidified in a Bridgeman furnace with a pulling velocity (*V*) of 30 μm/s and temperature gradient (*G*) of 10 to 20 K/mm. Then the cylindrical sample with a diameter of 6.6 mm was quenched into a Ga-In-Sn liquid metal and two samples were taken from just below the quench zone; one for sCT and the other for EBSD analysis. First, longitudinal sections were mechanically ground using SiC paper and then polished with 0.5-μm diamond suspension with ethanol as lubricant. Second, the surface oxide film and deformation layer were removed using focused ion beam (30 kv, 20 pA, FEI strata 235 Dual Beam) to obtain a high-quality diffraction pattern. Finally, EBSD analysis was performed on a FEI Quanta 200 FEG scanning electron microscope (30 kV, spot size ~1.5 nm) with the HKL system using a step size of 0.6 μm. Orientation maps were then analyzed to determine the crystallographic orientation of several primary trunks. The second portion from the quench zone was prepared for synchrotron X-ray tomographic imaging. sCT experiments were carried out at BL13W1 of the Shanghai Synchrotron Radiation Facility (SSRF, China), with a pixel size of 0.74 μm and 900 projections for each scan. The details of the SSRF experimental setup and parameters are similar to those described in Reference 15. The raw 3-D images were processed by *ImageJ* with a median filter and then *Avizo*@ (FEI, France) for 3-D rendering and quantification.

Three isolated dendritic grains were extracted out of the sample for examinations. Figure 1 provides the analysis results on one of these three primary α-Mg columnar dendrites which were quantified from the directionally solidified Mg-38wt pctZn alloy, imaged using sCT. Surprisingly, instead of the expected six-fold symmetry (shown schematic in Figure 1(a)[15,16]), the dendrite branches are observed to grow in an asymmetric manner with seven secondary arms evolving around the trunk (Figure 1(b)). Additionally, the seven secondary branches were found to grow with three distinct morphologies. The three morphologies are both qualitatively very different, as seen by comparing Figures 1(d) through (j), and quantitatively distinguishable via their growth angles to the primary, as shown in

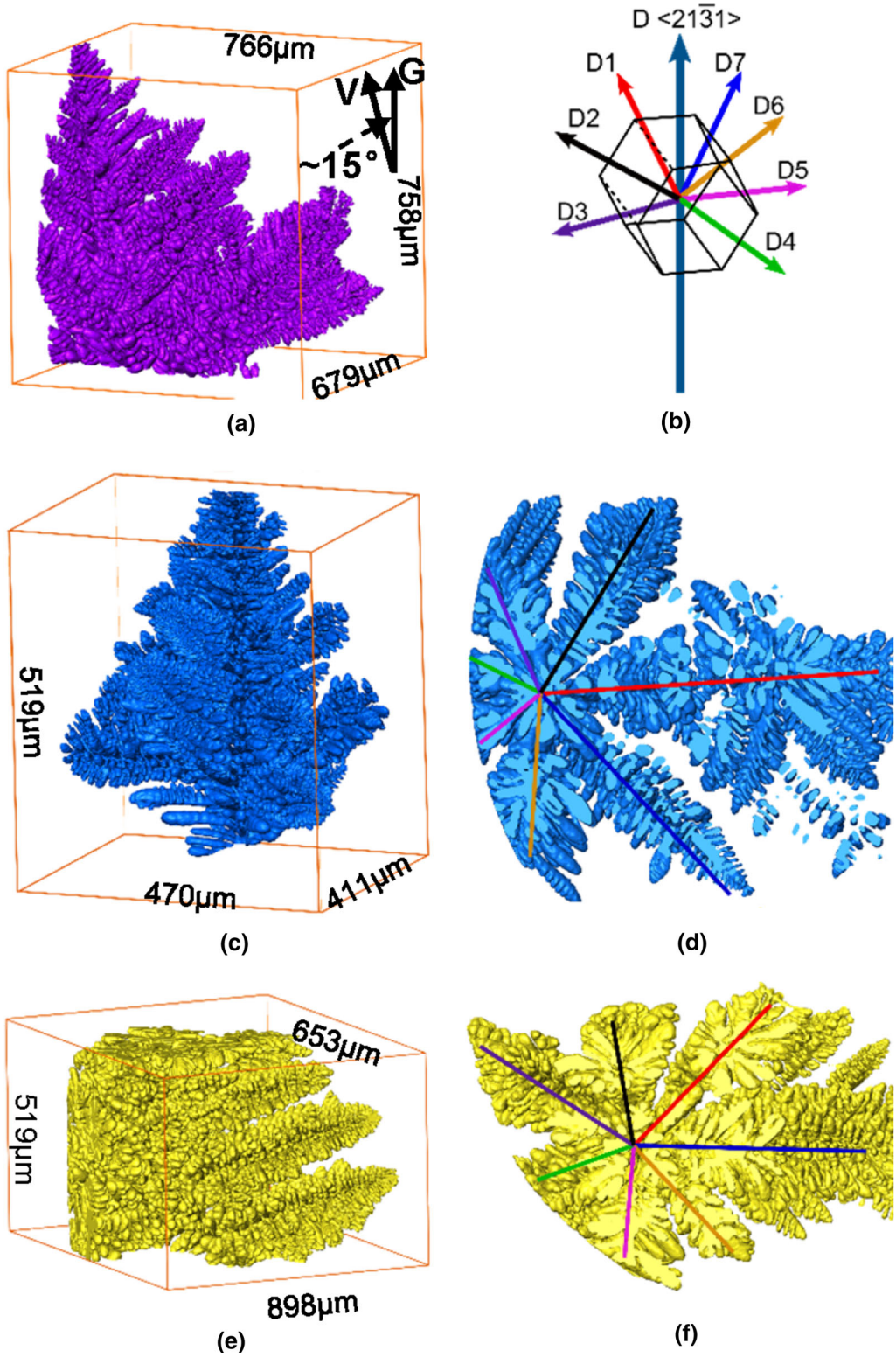

Fig. 3—(*a*, *c*, *e*) Three additional dendrites from DS Mg-38wt pctZn samples oriented in the vertical direction, which all display the same primary α-Mg dendrite growth direction ($\langle 21\bar{3}1\rangle$, shown schematically in (*b*) as the dendrite in Fig. 1. All three also had seven secondary arms, as shown in cross section for two in (*d*, *f*).

Table I (each average values is from at least six secondary arms along the trunk length) and discussed in detail below.

The first morphology we term *traditional*, with the arms growing in crystallographically favorable directions (*e.g.*, $\langle 4\bar{2}\bar{2}5\rangle$) with hierarchical tertiary branches

(Figures 1(d) (D1), (f) (D3), (i) (D6)). The angles are ~54 deg with respect to the trunk, and are qualitatively and quantitatively similar to those observed in prior high G/V directionally solidified Mg alloys with a $\langle 11\bar{2}0\rangle$ primary stem (*e.g.*, in AZ91[16]). This was the most prevalent morphology, occurring in just under half of the observed secondary dendrites in the Mg-38wt pctZn Bridgman-solidified sample.

The second morphology, termed *seaweed structure*, occurred on two of the arms (Figures 1(g) (D4) and h (D5)). The seaweed structure seems to grow with an angle of ~40 deg to the trunk initially, but then bends to a larger angle (~60 deg). Prior studies have observed seaweed-like structures during solidification either at near-isothermal conditions[24–27] or in deeply undercooled metallic melts.[28–30] Textured seaweed structures were also observed by Rappaz *et al*.[8–10,19] in aluminum alloys when zinc was added at compositions of 25 to 55 wt pct. Our results in Mg-Zn, combined with those of Rappaz *et al*. in Al-Zn, support Rappaz's hypothesis that the increase in interfacial energy anisotropy due to the addition of Zn alters the growth morphology. It is noted that the two seaweed-like arms, D4 and D5, are adjacent and it could be hypothesized that they started as one branch that divided via twining or tip splitting.

The third morphology, termed *free growth*, occurs when branches initially form at an angle of ~60 deg with respect to the primary but then bend away from the trunk, becoming almost perpendicular (Figures 1(e)(D2) and (j) (D7)). From the sCT images, it could be seen that the interdendritic spaces in front of these dendrites were much wider than for other secondary arms. We hypothesize that these curved dendrites have formed as a result of Zn solute being rejected during solidification, resulting in an increase in the Zn concentration in front of the growth interface, thus altering γ'_{sl},[9] and ultimately altering the growth direction. As solidification progresses, Zn will be partitioned, enriching in the interdendritic liquid and buoyancy may cause macrosegregation. Any resulting change in composition will modify the anisotropy; however, detailed examination of the secondary branch morphology along the entire sample shows little variation. Thus, the effect of gravity segregation seems to cause insignificant influence on the dendritic morphology during growth for this very small diameter sample. Although mechanical bending due to buoyancy has been suggested as a potential cause in other alloys,[31] here the α-Mg secondary dendrites arms lighter than the Zn-enriched liquid, and hence the forces are in the opposite direction, making this factor unlikely. In summary, prior studies have shown that the interplay of thermal conditions, solute diffusion, and interfacial free energy anisotropy is very complex, and all of these factors can influence dendritic growth,[32] resulting in a range of morphologies from the dendritic to seaweed like to fractural.[33,34]

The qualitative observations made in Figure 1 were verified through EBSD. Figure 2 shows an example of SEM micrograph, orientation map and corresponding pole figure resulting from the EBSD performed on the longitudinal section of the directionally solidified Mg-38wt pctZn. Instead of the frequently reported $\langle 11\bar{2}0\rangle$, $\langle 11\bar{2}1\rangle$, $\langle 11\bar{2}3\rangle$ or $\langle 22\bar{4}5\rangle$ orientations in Mg alloys,[15–18] the primary arms grew in a direction close to $\langle 21\bar{3}1\rangle$ which is between $\langle 11\bar{2}0\rangle$ and $\langle 22\bar{4}5\langle$ (about 22 deg to $\langle 11\bar{2}0\rangle$ and 35 deg to $\langle 22\bar{4}5\rangle$) was observed. Furthermore, all of the dendrites show the same unusual morphology of seven asymmetrical secondary arms evolving around a primary trunk (as shown in Figures 3(c) through (f) qualitatively, and quantitatively in Table I) that is growing in the $\langle 21\bar{3}11\rangle$ direction (as confirmed by EBSD on all dendrites in the section).

Note that although the orientation is approximate as it is difficult to section exactly parallel to the main trunk of dendrites when there is a tilt angle between the dendritic growth direction and the imposed temperature gradient (marked in Figure 2(a)). However, from the result depicted in Figures 2(a) and (b), the section plane appears to be nearly parallel to the main trunk, since the primary arm spans 80 pct of the micrograph in the vertical direction.[33]

In conclusion, synchrotron X-ray tomography has elucidated abnormal dendritic growth in directionally solidified Mg-38wt pctZn, both in terms of the primary arm growth direction ($\langle 21\bar{3}1\rangle$ rather than the previously reported $\langle 11\bar{2}0\rangle$ and $\langle 22\bar{4}5\rangle$ directions), and the asymmetry of the secondary arm side branches. Specifically, seven asymmetric secondary arms evolve behind each advancing primary rather than the expected six-fold symmetry.[15–17] These evolving sets of secondary dendrites in themselves showed three different morphologies: typical; seaweed-like structures; or free growth. All three morphologies were found to grow simultaneously on the same primary trunk. It was hypothesized that the combined influence of imposed thermal gradient and anisotropy in surface energy due to the Zn alloying addition caused this unusual structure to form, similar to the dendrite orientation transition hypothesized by Rappaz *et al*.[8–10] This demonstrated the influence of both composition and thermal conditions upon the morphology of dendritic microstructures formed during solidification.

This work is financially supported by the National Science Foundation of China (Grant Nos. 51175292 and 51404016), Postdoctoral Science Foundation of China (Grant No. 2014M550588), innovation platform for through process modeling and simulation of advanced materials processing technologies project (Grant No. 2012ZX04012-011). The analysis was performed in the Research Complex at Harwell, funded in part by the EPSRC (EP/I02249X/1), with S.S. provided financial support by the Chinese Scholarship Council. Authors would also gratefully acknowledge the Shanghai Synchrotron Radiation Facility for experimental support. Note, representative samples of the research data are shown in the figures/tables; however, the underlying raw data are not shared online due to its size.

REFERENCES

1. B. Mordike and T. Ebert: *Mater. Sci. Eng. A*, 2001, vol. 302, pp. 37–45.
2. K.U. Kainer: *Magnesium Alloys and Technologies*, Wiley, 2006, pp. 125–40.
3. T.M. Pollock: *Science*, 2010, vol. 328, pp. 986–87.
4. M. Asta, C. Beckermann, A. Karma, W. Kurz, R. Napolitano, M. Plapp, G. Purdy, M. Rappaz, and R. Trivedi: *Acta Mater.*, 2009, vol. 57, pp. 941–71.
5. M. Gündüz and E. Çadırl: *Mater. Sci. Eng. A*, 2002, vol. 327, pp. 167–85.
6. C. Puncreobutr, P.D. Lee, R.W. Hamilton, and A.B. Phillion: *JOM*, 2012, vol. 64, pp. 89–95.
7. D. Fuloria and P.D. Lee: *Acta Mater.*, 2009, vol. 57, pp. 5554–62.
8. T. Haxhimali, A. Karma, F. Gonzales, and M. Rappaz: *Nat. Mater.*, 2006, vol. 5, pp. 660–64.
9. J. Friedli, J.L. Fife, P. Di Napoli, and M. Rappaz: *Metall. Mater. Trans. A*, 2013, vol. 44A, pp. 5522–31.
10. F. Gonzales and M. Rappaz: *Metall. Mater. Trans. A*, 2006, vol. 37, pp. 2797–2806.
11. J.A. Dantzig and M. Rappaz: *Solidification*, EPFL Press, London, 2009, pp. 287–342.
12. M.Y. Wang, J.J. Williams, L. Jiang, F. De Carlo, T. Jing, and N. Chawla: *Scripta Mater.*, 2011, vol. 65, pp. 855–58.
13. M. Wang, T. Jing, and B. Liu: *Scripta Mater.*, 2009, vol. 61, pp. 777–80.
14. M. Wang, Y. Xu, Q. Zheng, S. Wu, T. Jing, and N. Chawla: *Metall. Mater. Trans. A*, 2014, vol. 45A, pp. 2562–74.
15. M.Y. Wang, Y.J. Xu, T. Jing, G.Y. Peng, Y.N. Fu, and N. Chawla: *Scripta Mater.*, 2012, vol. 67, pp. 629–32.
16. K. Pettersen, O. Lohne, and N. Ryum: *Metall. Trans. A*, 1990, vol. 21, pp. 221–30.
17. K. Pettersen and N. Ryum: *Metall. Trans. A*, 1989, vol. 20, pp. 847–52.
18. M. Yang, S. Xiong, and Z. Guo: *Acta Mater.*, 2016, vol. 112, pp. 261–271.
19. J.A. Dantzig, P. Di Napoli, J. Friedli, and M. Rappaz: *Metall. Mater. Trans. A*, 2013, vol. 44, pp. 5532–43.
20. R.E. Napolitano and S. Liu: *Phys. Rev. B*, 2004, vol. 70, p. 214 103.
21. R.E. Napolitano, S. Liu, and R. Trivedi: *Interface Sci.*, 2002, vol. 10, pp. 217–32.
22. D. Sun, M. Asta, J. Hoyt, M. Mendelev, and D. Srolovitz: *Phys. Rev. B*, 2004, vol. 69, p. 020102.
23. D.Y. Sun, M.I. Mendelev, C.A. Becker, K. Kudin, T. Haxhimali, M. Asta, J.J. Hoyt, A. Karma, and D.J. Srolovitz: *Phys. Rev. B*, 2006, vol. 73, p. 024116.
24. H. Emmerich, D. Schleussner, T. Ihle, and K. Kassner: *J. Phys. Condens. Matter.*, 1999, vol. 11, p. 8981.
25. N. Provatas, Q. Wang, M. Haataja, and M. Grant: *Phys. Rev. Lett.*, 2003, vol. 91, p. 155502.
26. B. Utter, R. Ragnarsson, and E. Bodenschatz: *Phys. Rev. Lett.*, 2001, vol. 86, p. 4604.
27. B. Utter and E. Bodenschatz: *Phys. Rev. E*, 2005, vol. 72, p. 011601.
28. K. Taguchi, H. Miyaji, K. Izumi, A. Hoshino, Y. Miyamoto, and R. Kokawa: *Polymer*, 2001, vol. 42, pp. 7443–47.
29. K.L. Beers, J.F. Douglas, E.J. Amis, and A. Karim: *Langmuir*, 2003, vol. 19, pp. 3935–40.
30. A.M. Mullis, K.I. Dragnevski, and R.F. Cochrane: *Mater. Sci. Eng. A*, 2004, vol. 375, pp. 157–62.
31. B. Billia, N. Bergeon, H.N. Thi, H. Jamgotchian, J. Gastaldi, and G. Grange: *Phys. Rev. Lett.*, 2004, vol. 93, p. 126105.
32. M.E. Glicksman: *Metall. Mater. Trans. B*, 2012, vol. 43, pp. 391–404.
33. M. Amoorezaei, S. Gurevich, and N. Provatas: *Acta Mater.*, 2012, vol. 60, pp. 657–63.
34. S. Gurevich, M. Amoorezaei, D. Montiel, and N. Provatas: *Acta Mater.*, 2012, vol. 60, pp. 3287–95.